International Journal of Material Forming, Volume 13, Issue 2, Pages 303 – 316 (1 March **2020**)

DOI: https://doi.org/10.1007/s12289-019-01487-2

Analysis of formability in conventional hole flanging of AA7075-O sheets: punch edge radius effect and limitations of the FLC

M. Borrego, D. Morales-Palma, A. J. Martínez-Donaire, G. Centeno, C. Vallellano*

Dept. Mechanical and Manufacturing Engineering, University of Seville, Spain

**corresponding author: carpofor@us.es*

Abstract

Hole flanges are commonly manufactured in mass production by conventional press-working. In an industrial context, the process limits are usually evaluated by means of the Limiting Forming Ratio (*LFR*), which defines the maximum attainable diameter of the flange related to the initial pre-cut hole. Nevertheless, the *LFR* does not provide enough information about material deformation, thickness distribution or the expected onset and type of failure. In this sense, a systematic investigation using the Forming Limit Diagram (FLD) is needed. Under these circumstances, the aim of this work is to provide a better understanding of the deformation process in conventional hole flanging, analysing the effect of the punch edge radius as well as the influence of the strain distribution along the hole flange on formability. An experimental campaign on 1.6 mm thickness AA7075 annealed sheet was completed using cylindrical punches with different profile radii. In addition, numerical modelling of the process using finite elements was developed. The results allow better understanding of the physical mechanisms governing material deformation and process formability in very ductile materials. In this regard, this research work contributes to the current state of the art in conventional hole flanging by establishing the modes of failure that prevail in the process and the influence of the bending induced by the tool radius in the flange formability. In addition, the limitations of using conventional FLD for providing a limiting threshold for the strain states attained in the flanges deformed with different punch profiles are also identified.

Keywords: Hole flanging, Formability, Forming Limit Diagram, Necking, Bending.

1. Introduction

Hole flanging by press-working is a conventional sheet forming process where a clamped blank with a pre-cut hole is deformed in a single punch stroke. The material around the hole is forced to expand, being subjected to a combination of circumferential stretching and meridional bending. Typical industrial applications of those circular-lip components pursue to stiffen the edges of the holes, to improve their appearance or to provide additional support for press fitting or welding for joining sheet parts to tubes.

Given the industrial importance of hole flanging, this forming process has attracted the interest of several researchers. Yamada and Koide [1] numerically analysed the results of bore-expanding tests with cylindrical punches using the incremental theory of plasticity. Johnson et al. [2] investigated the hole-flanging process with conical punches and analysed the deformation process and influence of the material anisotropy on the failure at the flange edge. Using finite

element analysis (FEA), Tang [3] studied flange formation with four different punch shapes (hemispherical, ellipsoidal, nearly flat and conical frustum) and concluded that the strain path at the flange tip during the forming process is independent of the punch shape, as well as the maximum strain at the flange edge, for an equal hole size and flange height. In more recent studies, Levy and Tyne [4] analysed experimental data of hole expansion tests of advanced high-strength steels (AHSS) sheets using conical and flat punches and observed a slightly increase of the calculated maximum strain at the hole edge with the conical punch. Similar conclusions were found by Pathak et al. [5], who explained that these differences in terms of formability are due to the differences in the strain states accomplished in each test: near-plane-strain conditions away from the hole edge for the flat punch, and edge failure under uniaxial tension for the conical punch. Kumagai and Saiki [6] investigated the hole flanging with ironing of thick sheet metals, pointed out that the punch load and the finished shape could be predicted accurately by the rigid-plastic FEA. Leu et al. [7] used a finite-element method based on Lagrangian formulation to predict the limiting condition of hole flanging for three punch shapes (cylindrical, conical and spherical). They proposed that the critical thickness of the hole edge for necking for all three punch shapes was the same as the fracture thickness of the material under simple tension conditions.

In practice, the hole expansion ratio (*HER*), defined as the ratio of the inner diameter (d_f) of the finished flange to the initial hole diameter (d_0), quantifies the deformation in circular hole-flanging. The maximum value attainable by the material without failure is called the limiting forming ratio (*LFR*), which is defined as follows:

$$LFR = \frac{d_{f,max}}{d_{0,min}} \tag{1}$$

where $d_{f,max}$ *and* $d_{0,min}$ are, respectively, the maximum inner diameter in the finished part and the minimum pre-cut hole of the blank. Huang and Chien [8,9] studied numerically and experimentally the *LFR* of a hole-flanging process for low-carbon sheets using various cylindrical punch profile radii. As usual for conventional hole flanging, the *LFR* was evaluated assuming $d_{f,max}$ to be the punch diameter. They noted that the *LFR* is independent of the punch radius. However, the punch profile definitely has a great influence on the final flange shape and maximum punch force of the process. They observed that the maximum reduction in the wall thickness occurs along the periphery of the expanded hole. Thus, failure at the edge of the flanged hole is controlled by the tensile stress in the circumferential direction.

In addition to the initial pre-cut hole size and punch shape, other process parameters that affect the final flange include the blank-holding force, as analysed by Krichen et al. [10], the clearance between the punch and the die, and the material anisotropy, as investigated by Kacem et al. [11,12]. As reported in these studies, the punch-die clearance seems to be an influential factor as far as, depending on its value, ironing could develop. Soussi et al. [13] analysed the conventional hole-flanging process using 1000-series aluminium alloy sheets of 0.8-mm thickness and varying the initial pre-cut hole diameter and the clearance to thickness ratio. A failure map of the flanging process involving the process parameters and the geometry was proposed as a tool for product design. Moreover, the recent works of Yoon et al. [14,15] discuss the key factors governing the hole expansion ratio of sheet materials, pointing out that the fracture toughness, measured using the fracture initiation energy, could be an universal factor governing stretch-flangeability.

In some materials, especially in high strength materials or low ductility materials, the events of initiation of necking and subsequent fracture may be very close or necking may be suppressed. Some researchers have observed the onset of cracks without previous necking at the hole edge in double phase (DP) steel and AHSS sheets, as pointed out by Pathak

et al. [5] and Wang et al. [16], respectively. Pathak et al. [5] concluded that this might be due to such steels exhibiting low resistance to fracture at the onset of localized necking.

On the other hand, the conventional Forming Limit Curve (FLC) is currently the most useful tool for evaluating the formability of metal sheets during the design process of press-working operations and provides the limit strains at the onset of localized necking. However, most studies on hole flanging have been devoted to analysing the sheet formability via the *LFR* or related parameters. Among others, Martins and co-workers used the FLC to compare the formability of flanges fabricated by press-working and single-point incremental forming using different materials [17-19]. In general, very few works have used the FLC as an analysis tool, and these works have not provided a detailed description of the flange deformation process or a deep study on the influence of the punch profile.

The aim of this work is to contribute to the comprehension of the factors that control the formability of the sheet during hole-flanging operations using conventional press-working. The deformation process of the flange and the influence of the initial hole size and punch profile in the failure and final geometry of the flange are discussed in detail. To this end, a set of experimental tests using 1.6 mm thickness sheets aluminium alloy 7075-O were performed and analysed using 3 different cylindrical punches with different profile radii (10, 8 and 6 mm) and a hemispherical punch. The distribution of principal strains along the flange was measured using an optical 3D forming analysis system (ARGUS®). The formability of the flange was analysed via the traditional *LFR* and conventional FLC. The results show that the conventional FLC presents limitations for the evaluation of the material formability along the flange wall. Besides, the actual influence of the bending effect induced by the punch radius as well as the apparent independence of the punch profile on the flange formability are clearly elucidated.

2. Experimental procedure

2.1. Mechanical characterisation

The experimental work was carried out in aluminium alloy 7075-O sheets of thickness 1.6 mm. The mechanical characterization of the material at 0°, 45° and 90° with respect to the sheet rolling direction was carried out by means of tensile tests (see Figure 1). The tests were performed at room temperature in an INSTRON 1125 testing machine, following the standard ASTM E8. Mechanical properties are given in Table 1.

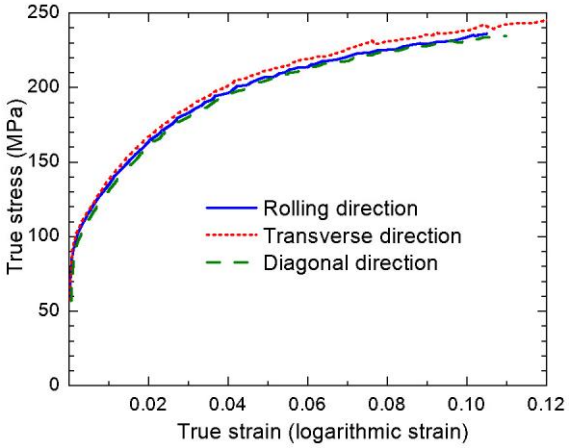

Figure 1. True stress–strain curves of tensile tests in three directions for AA7075-O sheets of thickness 1.6 mm.

Table 1. Mechanical properties of AA7075-O sheets (standard deviation in brackets)

Sheet direction	*E* [GPa]	*YS* [MPa]	*UTS* [MPa]	e_f [%]	*r*
Rolling (0°)	69.7 (1.1)	110 (0.5)	214 (0.5)	20.6 (0.025)	0.65 (0.01)
Diagonal (45°)	66.7 (0.9)	108 (0.4)	212 (0.5)	19.6 (0.021)	0.97 (0.06)
Transverse (90°)	74.1 (1.4)	112 (0.5)	218 (0.5)	17.7 (0.022)	0.81 (0.04)
Average $(x_0 + 2x_{45} + x_{90})/4$	69.5 (1.3)	109 (0.5)	214 (0.5)	19.4 (0.019)	0.85 (0.03)

E: modulus of elasticity; *YS*: yield strength; *UTS*: ultimate tensile strength; e_f: total elongation; *r*: Lankford coefficients.

The Lankford coefficients (*r*-values in Table 1) were obtained according to the standard ASTM E517. They were measured at a true strain level near, but not exceeding, the strain at the maximum applied force. In this case the plastic strain was set about 0.11.

2.2. Formability limits

The characterisation of the formability limits by necking and fracture of the AA75075-O sheets was developed in a previous work [20]. In this regard, a series of Nakazima tests in an Erichsen 142-20 testing machine was carried out according to the standard ISO 12004-2:2008. Different specimen geometries were tested to evaluate the sheet failure at different strain paths ranging from uniaxial to biaxial stretching. The friction was minimized by a combination of 2 polytetrafluoroethylene (PTFE) sheets of 0.05 mm in thickness and Vaseline. The punch speed was set to 1 mm/s and the specimen deformation was continuously recorded by the DIC system ARAMIS®.

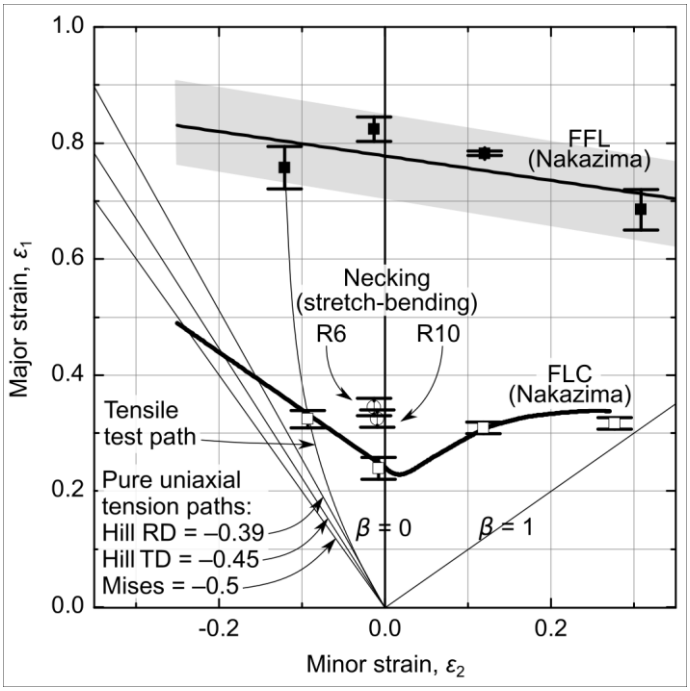

Figure 2. Forming limit diagram (FLD) representing the conventional formability limits at necking and fracture (FLC and FFL) as well as the forming limits at necking in stretch-bending conditions using cylindrical punches of radius 6 and 10 mm.

The experimental FLC for necking and Fracture Forming Limit (FFL) are shown in Figure 2. The former was obtained according to the time-dependent methodology for detecting the onset of localized necking proposed by Martínez-Donaire et al. [21]. The FFL was determined in post-mortem specimens by directly measuring under a microscope the sheet thickness at the fracture onset point on both sides of the crack, which was accurately determined by analysing the images recorded by ARAMIS. At least three tests were performed for each specimen geometry (uniaxial tension, near plane-strain, biaxial and equi-biaxial strain). The measurements were validated by cutting some specimens perpendicularly to the crack and measuring the thickness in the profile view. The principal strains at fracture (ε_{1f}, ε_{2f}, ε_{3f}) were then calculated from thickness measurements by assuming volume constancy and a local plane strain state from necking up to fracture. The minor principal strain at fracture (ε_{2f}) was estimated as the average value of ε_2 measured using ARAMIS along the fracture line at the last image recorded, just before the crack appearance. The experimental 10% scatter bar around the average values of fracture strains is also depicted in Figure 2.

A series of stretch-bending tests under near-plane-strain conditions were also conducted using cylindrical punches with radii of 10 and 6 mm. The experimental setup and test procedure was described by Martínez-Donaire et al. [21] for a different batch of the same material. The necking strains were obtained using the same methodology described above for the Nakazima tests and are shown in Figure 2 along with their experimental scatter. The stretch-bending tests enabled a controlled bending through the sheet thickness in the failure region and they will be used later to assess the influence of the punch profile in conventional hole flanging.

Figure 2 also depicts the strain path of Nakazima tests in uniaxial tension, the linear strain paths according to Mises ($\beta = -0.5$) and Hill'48 anisotropic yield criteria in the rolling direction ($\beta = -r_0/(1+r_0) = -0.39$) and the transverse direction ($\beta = -r_{90}/(1+r_{90}) = -0.45$), as well as plane-strain ($\beta = 0$) and equi-biaxial stretching ($\beta = 1$). Notice that, except at the

very begining of the tests, the experimental strain path in the tensile tests differs notably from the theoretical strain paths in pure uniaxial tension conditions due to the specimen geometry. These theoretical strain paths in pure uniaxial tension will be used later to assess the influence of the material anisotropy on the edge deformation of hole-flanged parts.

2.3. Hole-flanging tests

Table 2 shows the plan of the experiments. It also includes a schematic representation of the hole-flanging operations using conventional press-working. The tests were carried out using an Erichsen 142-20 machine with a blank holder and a 100-mm diameter die. The blanks were cut out from the supplied sheets of AA7075-O with a 1.6-mm thickness. The blanks were circular, with an external diameter of 180 mm and central pre-cut holes with different diameters (d_0) (see Table 2). The central holes were milled and subsequently ground with fine grit sandpaper to eliminate any burrs.

Table 2. Experimental plan. Scheme of hole-flanging operation using conventional press-working

Pre-cut diameter hole, d_0 (mm)	*Die diameter (mm)*	*Punch diameter, D_p (mm)*	*Edge radius R (mm)*	
35				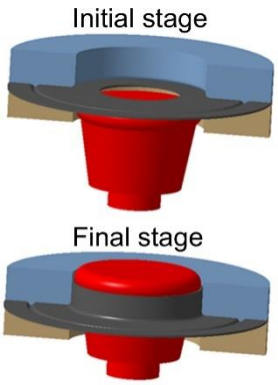
41				
58			6	
59			8	
60	100	95.8	10	
61			47.9	
65				
72				
83				

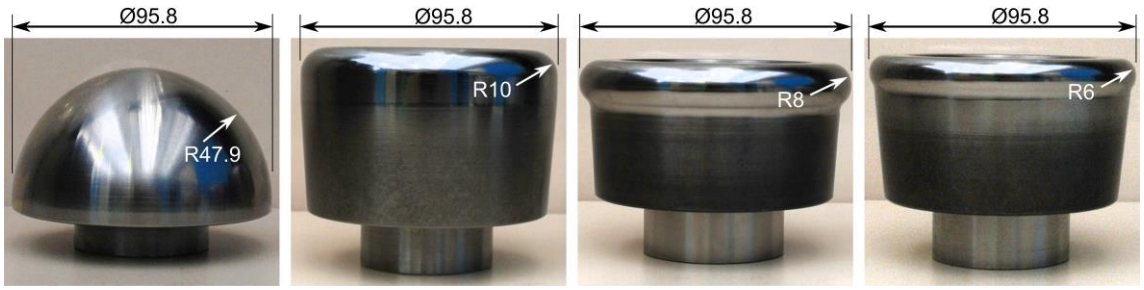

Figure 3. Set of punches with different edge radii for hole-flanging tests (6, 8, 10 and 47.9 mm).

A series of punches with an equal circumferential diameter (D_p) and different edge radii (R) was used to analyse the effect of the punch profile on the formability. A circumferential diameter of 95.8 mm and four edge radii of 6, 8, 10 and 47.9 mm (hemispherical punch) were selected (see Figure 3). The gap between the die and punch was slightly bigger than the sheet thickness to avoid ironing during the forming process. The die, blank holder and punches were made of UNE F1430 steel, subsequently tempered and hardened up to 60 HRC. Furthermore, punches were lapped to minimise friction.

As shown in the scheme of Table 2, during the flanging process, the punch deforms the material around the pre-cut hole in the blank to form a hollow flange. The operation attempts to achieve the final flange with a single pass of the tool and is successful when a complete flange that is free of defects is obtained. The punch speed was set to 1 mm/s. The contact between the blank and punch was lubricated with Vaseline. The blank-holding force was set to 85 kN, which was sufficiently high to avoid the blank from drawing-in. According Krichen et al. [8], the blank-holding conditions do not influence the maximum punch load, but an insufficient holding force may modify the finished flange due to springback effects. Therefore, it is always advised to use a holding force that is higher than the maximum reaction force experienced by the punch during the test.

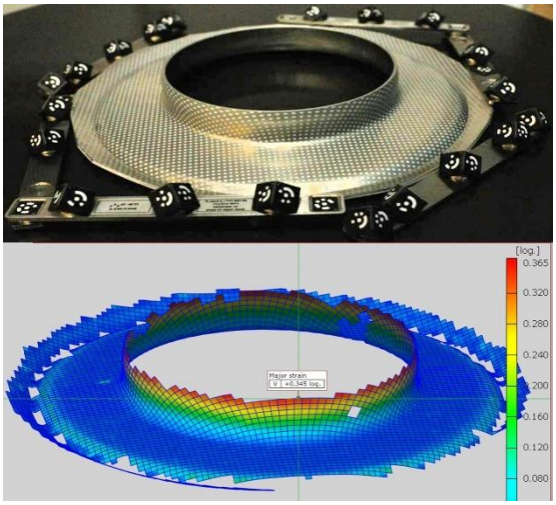

Figure 4. Specimen after testing showing the grid of circles (up) and contour of in-plane principal strains measured using ARGUS (down).

The strain distribution at the outer surface of the specimen were measured using circle grid analysis. Blanks were previously electro etched with a grid of circles of 1 mm diameter and spaced at 2 mm from centre-to-centre. The ARGUS system was used to compute the principal strains at the outer surface. Measurements were performed once the flange successfully finished or right after its failure. Figure 4 illustrates the circle grid analysis for a successful specimen. As can be seen, the software is not able to compute the strains at edges. Thus, in this work, the in-plane principal and thickness strains at the hole edge were obtained by measuring the final and initial diameter of the hole and the sheet thickness, respectively, and assuming volume constancy:

$$\varepsilon_1 = ln\frac{d_f+2t}{d_0}, \varepsilon_3 = ln\frac{t}{t_0}, \varepsilon_2 = -(\varepsilon_1 + \varepsilon_3) \quad (2)$$

Finally, the final flange height was also obtained to quantify the geometric capabilities of the process. Dimensions were measured using a digital caliper Mitutoyo CD 15APX with a resolution of 0.01 mm.

3. Results and discussion

In this section, the tests results are described and a critical analysis of the formability based on the *LFR* and the conventional FLC is presented. The influence of the punch profile on the deformation of the flange is discussed.

3.1. Tests results

Table 3 summarises the results of the experimental campaign shown in Table 2. The different punches are identified by their edge radius (R). The label "*O*" indicates a successful test, that is, the hole-flanged part was obtained free of defects; "*N*" indicates tests that exhibited necked without fracturing the flanges; and "*F*" indicates specimens with fractured flanges. A series of increasing values of d_0 was tested to determine the successful flanges. Intermediate pre-cut holes were explored until a difference equal or less than 1 mm in diameter was reached between the successful and failed tests. The necking situations were verified using at least two different tests.

Table 3. Series of conducted hole-flanging tests

Edge radius, R (mm)	*Initial pre-cut hole diameter, d_0 (mm)*								
	35	41	58	59	60	61	65	72	83
6	*F*		*F*	*F/N*	*N*	*O*	*O*	*O*	*O*
8		*F*	*F*	*F/N*	*N*	*O*	*O*	*O*	*O*
10			*F*	*F/N*	*N*	*O*	*O*	*O*	*O*
47.9			*F*	*F/N*	*N*	*O*	*O*	*O*	*O*

Note: *F* - fractured flange; *N* - necked flange; *O* - successful flange

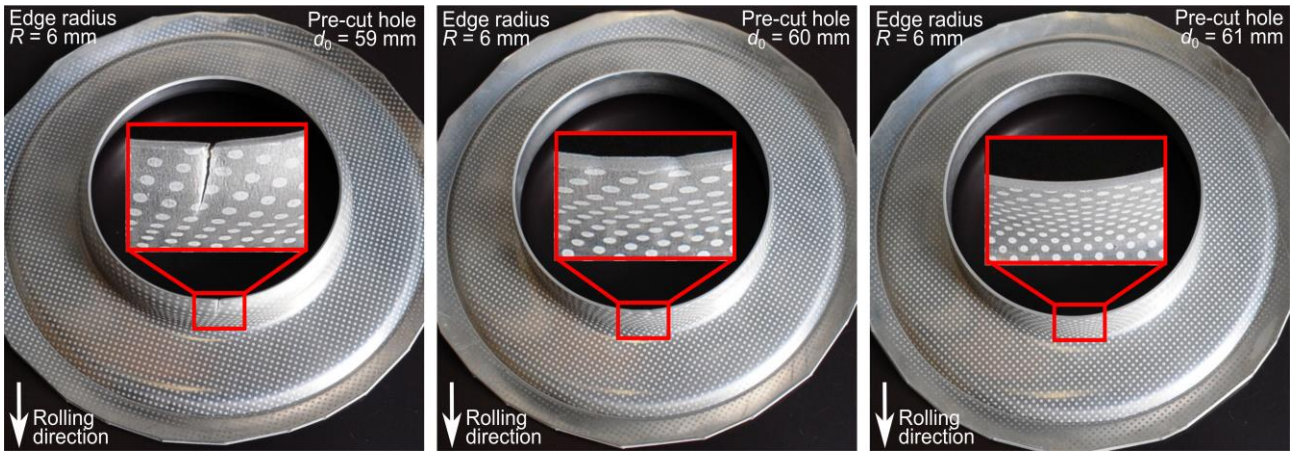

Figure 5. Flanges from pre-cut hole diameters of 59 (fractured), 60 (necked) and 61 mm (successful) with a 6 mm edge radius.

Figure 5 shows tests for the pre-cut holes with a 59, 60 and 61 mm diameter using a punch with a 6-mm edge radius. A successful flange was obtained for d_0 equal to 61 mm, whereas incipient necking at the hole tip was observed for d_0 equals to 60 mm and a meridional crack was clearly developed for d_0 equals to 59 mm. The mode of failure observed in all situations was the initiation of a neck at the edge of the flange, previous to the fracture of the material. The onset of localized necking appeared preferentially oriented along the rolling direction, as showed in Figure 5.

Table 4. Experimental results and process parameters of successfully formed specimens.

Edge radius, R (mm)	*d_0 (mm)*	*$d_f \approx D_p$ (mm)*	*h (mm)*	*Bending ratio t_0/R*	*HER (d_f / d_0)*	*LFR (d_f / $d_{0,min}$)*
6	61	95.8	18.2	0.27	1.57	1.57
6	65		16.4		1.47	
6	72		13.2		1.33	
6	83		7.6		1.15	
8	61	95.8	18.2	0.20	1.57	1.57
8	65		16.4		1.47	
8	72		13.0		1.33	
8	83		7.7		1.15	
10	61	95.8	18.2	0.16	1.57	1.57
10	65		16.5		1.47	
10	72		13.0		1.33	
10	83		7.7		1.15	
47.9	61	95.8	17.6	0.03	1.57	1.57
47.9	65		15.9		1.47	
47.9	72		12.9		1.33	
47.9	83		7.7		1.15	

Table 4 presents the geometric parameters checked in the successful parts of the different pre-cut holes. For the calculation of the *HER*, the final hole diameter (d_f) was assumed to be the punch diameter (D_p) which differed slightly due to springback. The bending ratio (t_0/R), defined as the ratio of the initial sheet thickness to the punch corner radius that quantifies the severity of local bending induced on the sheet thickness, is also presented. It should be noted that, except for the hemispherical punch, the flange height (h) values were nearly identical for a given pre-cut hole (d_0) when the bending ratios ranged from 0.16 to 0.27.

It should be noticed that there were no significant differences in the measurements of flange height (h) and thickness (t) along the circumferential perimeter of the edge. This is attributed to the material not differing strongly from an isotropic behaviour. Regarding the material anisotropy, the sheet thickness along the perimeter of the hole edge can be theoretically evaluated from the Lankford coefficients (Table 1). For instance, considering the hole-flanging operation of the blank sheet with a pre-cut hole diameter of 61 mm, the major strain is $\varepsilon_1 = \ln(95.8/61) = 0.451$ and, by volume

constancy, the thickness strain is $\varepsilon_3 = -(1+\beta)\,\varepsilon_1$. Given that $\varepsilon_3 = \ln(t/1.6)$, the theoretical thickness can be evaluated for different β-values. Using the Hill yield criterion, the sheet thickness calculated in rolling direction ($\beta = -0.39$) and transverse direction ($\beta = -0.45$) yields 1.248 and 1.215 mm, respectively. However, the hole edge was pressed by the punch at the last stages of the process and, therefore, the thickness may be slightly altered. Thus, the small differences in theoretical thickness (0.033 mm) and the contact effect, along with the experimental scatter, explain why the material anisotropy could not clearly be assessed.

3.2. Formability analysis based on the LFR

As explained in the introduction, *HER* measures the forming severity during conventional circular hole flanging and *LFR* the material formability. They are defined here as follows:

$$HER = \frac{D_p}{d_0} \therefore LFR \coloneqq \frac{D_p}{d_{0,min}} \tag{3}$$

Table 4 shows the values of the *HER* and *LFR* for the successful tests. The *LFR* remained constant with *R* and was equal to 1.57, indicating that the punch profile did not significantly influence successful flange formation, i.e., the flange formability. Similar conclusions have been noted by other authors, e.g., Leu et al. [5] and Huang et al. [6]. In their works, they noted that the formability during hole-flanging processes appeared to be unaffected by the punch profile. Nevertheless, the final shape of the flange was clearly influenced by the punch shape, mainly due to the springback that always occurs after flanging. The maximum punch force increased remarkably with the decrease in the punch profile radii.

The condition for the onset of localized necking at the hole tip must be fulfilled in the FLD (see Figure 2) at the intersection of the FLC with the line of pure uniaxial tension. Accordingly, the *LFR* value must be also intrinsically associated with this intersection point, and it can be expressed as a function of the limiting major strain at the onset of localized necking in pure uniaxial tension ($\varepsilon^*_{1,UT}$) as follows,

$$\varepsilon_1|_{holetip} = ln\left[\frac{\pi D_p}{\pi d_{0,min}}\right] = ln[LFR] \coloneqq \varepsilon^*_{1,UT} \therefore LFR \coloneqq e^{\varepsilon^*_{1,UT}} \tag{4}$$

As discussed later, the material at the hole tip is free of the influence of punch bending, which agrees with the fact that the *LFR* is a material constant and independent of the punch edge radius. This result is in full agreement with the results of Huang and co-workers [5,6], except for the fact that they adopted the fracture strain of the simple tension test as a necking criterion at the flange tip, instead of using the necking strain itself as proposed here. Given that the neck and subsequent crack propagated in the almost finished hole-flanged part along the rolling direction (RD, as can be seen in Figure 5), the flange edge in this zone was is subjected to uniaxial tension conditions in transverse direction (TD). As shown in Figure 2 and according to Eq. (4), a value of major strain at necking in uniaxial tension $\varepsilon^*_{1,UT}$ of 0.44 (Hill'48 in TD) or 0.47 (Mises) yields a *LFR* value of 1.55 of 1.60, respectively, which are in very good agreement with the experimental value of 1.57.

The above equation can be generalised to a wider range of β-values along the FLC (see Figure 2) in order to allow using the experimental thickness at necking measured in a tensile test:

$$LFR := e^{\frac{-\varepsilon_{3,UT}^{*}}{1+\beta^{*}}} = \left(\frac{t^{*}}{t_0}\right)^{\frac{-1}{1+\beta^{*}}} \tag{5}$$

where $\varepsilon_{3,UT}^{*}$ and t^{*} are the limiting thickness strain and the critical thickness at the onset of localized necking in pure uniaxial tension, and β^{*} is the strain ratio in pure uniaxial tension, accounting for material anisotropy. Note that the limiting thickness strain at the onset of localized necking (ε_3^{*}) in the left hand side of the FLC is assumed to be a material constant, thus Eq. (5) provides an estimation of the LFR in ductile materials just based on material properties.

3.3. Formability analysis based on the FLC

The conventional FLC is currently the most useful and used tool during the design stage of press-working operations for evaluating the formability of the metal sheet. In general terms, a safe operation is warranted when the strains in the sheet are well below the FLC.

Figure 6 shows the in-plane principal strain at the outer surface of the flange along the meridional direction in all successful finished specimens, i.e., the holed blanks of 61, 65, 72 and 83 mm diameter formed with the cylindrical punches and the hemispherical one. The inspection directions were oriented along the rolling direction, according to the preferential failure orientation. The principal strains computed using ARGUS are represented by a solid line and cover points from the base to nearly the edge of the flange. The strain at the exact flange edge at the outer sheet surface, obtained using direct measurement as indicated in section 2.3, is depicted with a star. As can be observed for all experimental tests, it did not exactly follow the pure uniaxial tensile path (neither $\beta = -0.45$ nor -0.5) mainly due to the experimental scatter, as explained above. The gap between the last point measured using ARGUS and the hole tip is depicted by a dotted line, and it was estimated to be approximately 1 mm. The major and minor strain directions correspond, respectively, to the circumferential and meridional direction of the part, i.e., the directions along and across the flange. As seen in Figure 6, the in-plane principal strain displays a 2-shaped curve. The strain initially shows significant contraction in the meridional direction, due to the bending of the flange around the die radius, followed by stretching of the flange wall in the circumferential direction and ending in pure uniaxial tension at the exact flange edge.

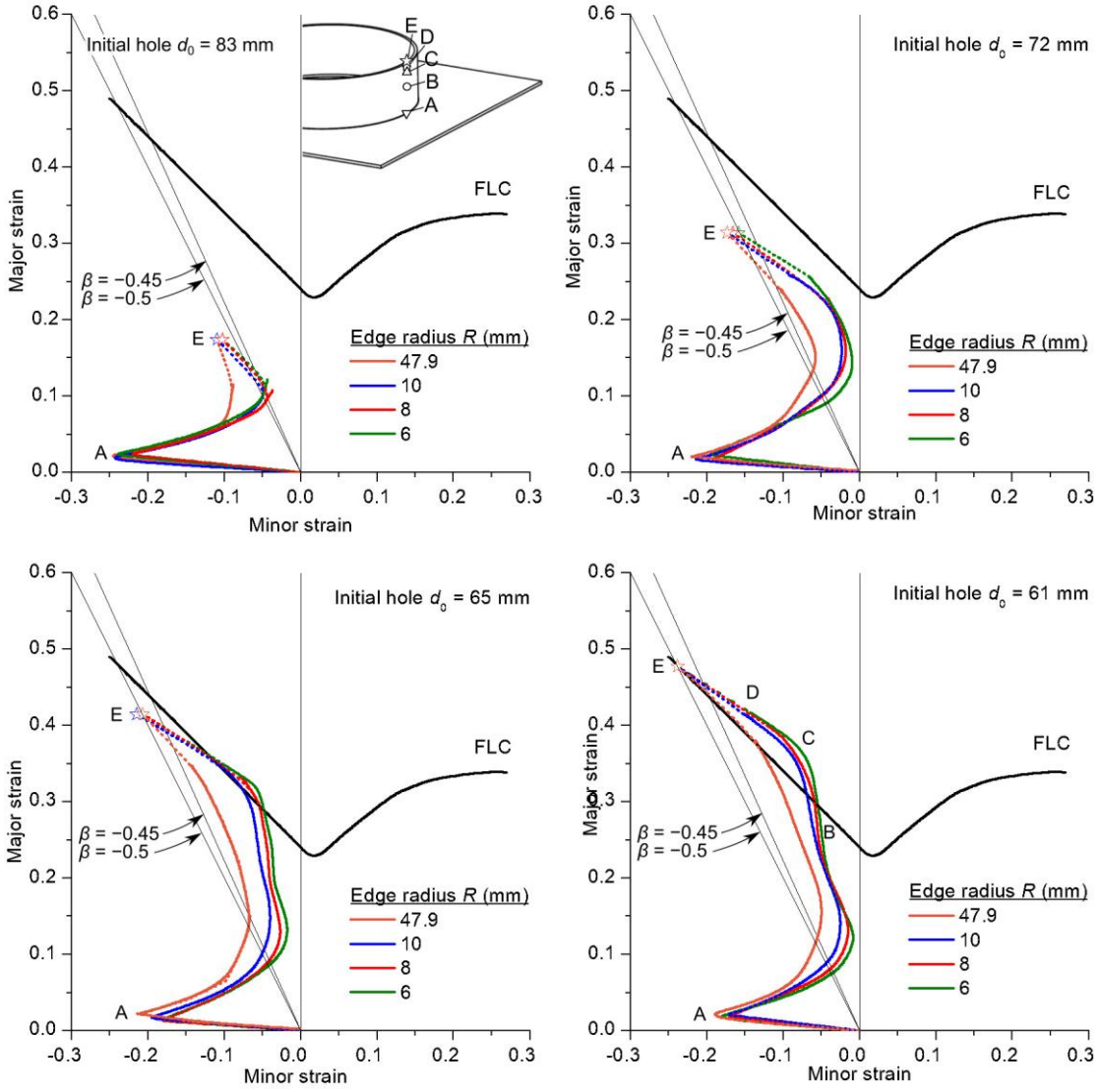

Figure 6. In-plane strain distribution along the meridional direction for successful specimens formed using punches with different edge radii (R).

In the hole-flanging process, the punch edge radius notably affected the meridional strain, i.e., the minor principal strains along the flange. Thus, the smaller the punch corner radius is, the higher the minor strain is. This fact produces a shift in the strain curves to the right in the principal strain diagram. This can be clearly observed in Figure 6, which compares the strain curve for the hemispherical punch and those for the cylindrical punches. The differences between the cylindrical punches are less apparent due to the experimental scatter. This shift is also responsible for the lower value of the flange height exhibited by the semi-spherical punch (see Table 4).

The most remarkable fact noted in Figure 6 is that, except for the hemispherical punch, the strain distributions for the pre-cut hole with a 61-mm diameter are clearly above the FLC. According to the traditional analysis using FLC, these parts should have failed at some point along the flange. However, this did not occur. This phenomenon of exceeding the FLC without failure when analysing conventional hole flanging can also be observed in the experimental works of

several researchers, such as Silva et al. [17] for Ti6Al4V and Montanari et al. [18] and Cristino et al. [19] for AISI304L, but it has not yet been analysed.

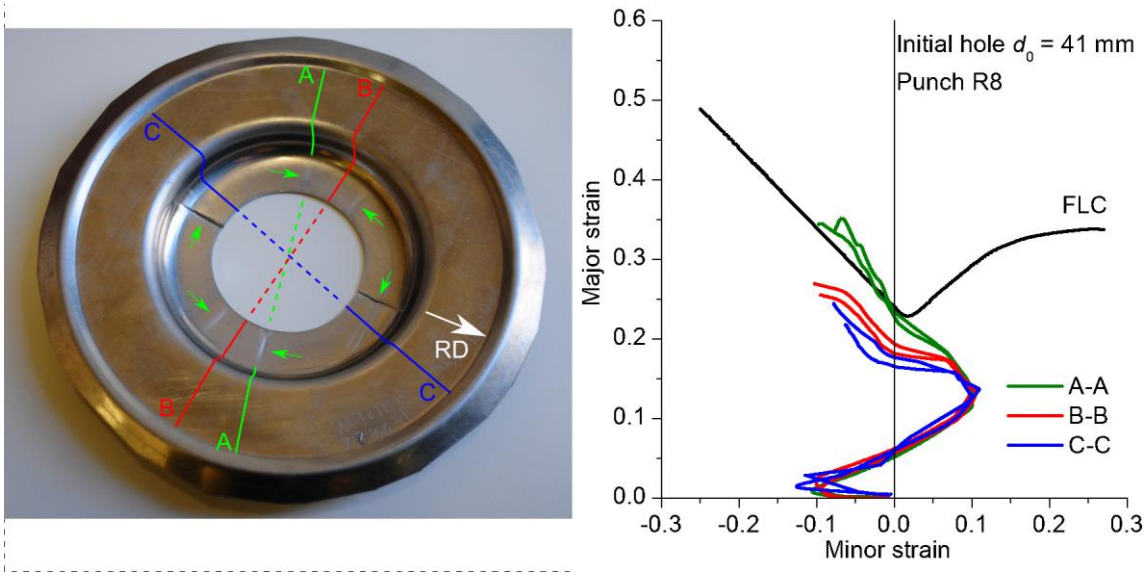

Figure 7. Bottom view of failed specimen showing necking and cracks formed in several directions (left) and strain distributions measured with ARGUS along different sections (right).

The expected failure in the specimens above did occur in those with smaller holes presented in Table 3 (d_0 = 35 and 41 mm). Figure 7 (left) shows the bottom view of a failed specimen of 41-mm pre-cut hole diameter tested with the punch of radius 8 mm. The green arrows point to the crack initiation site within the necked region in RD, as well as the appeared necks in 2 different directions near TD. All necks initiated away from the flange edge. Figure 7 (right) depicts the strain distributions measured with ARGUS along 3 different sections along the meridional direction. The strains just by the hole edge are not represented for this specimen. As expected, the material on the neck overcame the FLC (top of line A-A) and the material outside the failure zones remained below the FLC (bottom of line A-A and lines B-B and C-C). Similar observations were reported by Pathak et al. [5] for AHSS sheets, who found that failure initiated in near-plane-strain conditions.

As a result, it can be said that, in general terms, the conventional FLC seems not to be the right tool for describing the failure in hole flanging by press-working. Besides, a further analysis is required to explain the aforementioned phenomenon of successful flanges exceeding the FLC without failure (see Figure 6, specimens with d_0 = 61 mm). Two aspects of the deformation history are a priori candidates for explaining this observation: on the one hand, the non-proportionality of the strain paths during the deformation process and, on the other hand, the local bending induced by the punch edge radius in the flange.

3.3.1 *Effect of the strain path*

The strain path has a strong influence on the onset of localized necking. Experimental studies by Graf and Hosford [22] and Stoughton and Yoon [23] and theoretical/numerical studies by Barata da Rocha et al. [24] and Yoshida et al. [25] have shown that changes in the strain path significantly affect the shape and location of the FLC.

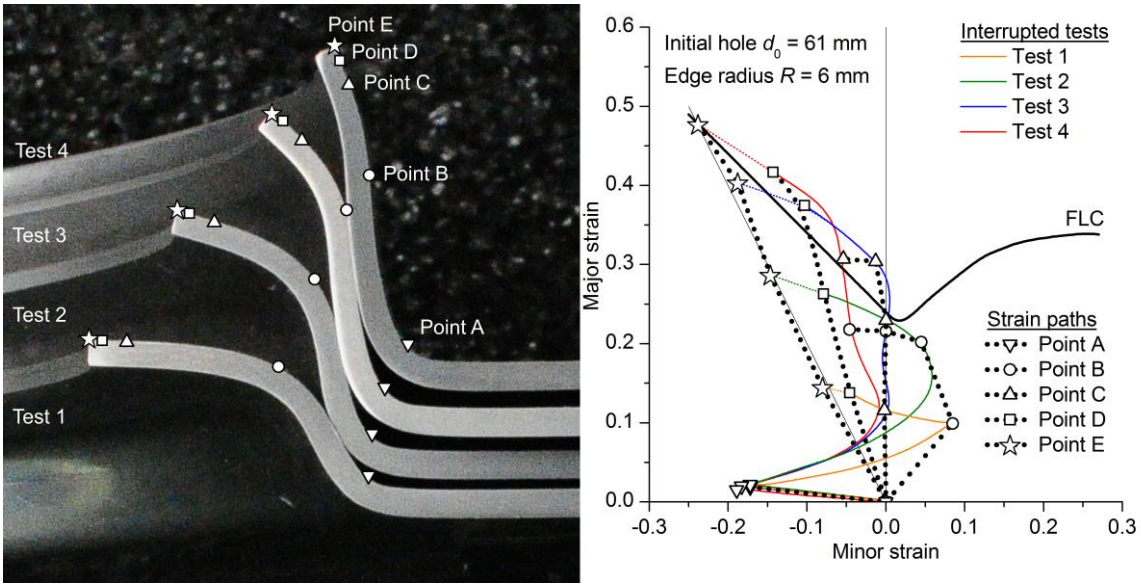

Figure 8. In-plane strain paths during the hole-flanging process obtained from the interrupted tests using the pre-cut hole of diameter 61 mm and a 6-mm punch edge radius.

To analyse the strain paths during flange formation, a given blank with the same pre-cut hole was tested, and the punch stroke was interrupted at different heights. Figure 8 (left) shows the flange for four interrupted tests using a pre-cut 61-mm hole and a cylindrical punch with a 6-mm edge radius.

The principal strains were measured at the end of each test, and the strain history at five points (A-E) along the meridional direction of the flange is represented in Figure 8 (right). The strains calculated by ARGUS were corroborated using a digital microscope. Point E, located at the hole tip, underwent uniaxial tension and grew linearly and proportionally from the origin to the final stage. Points D and C, located in between the hole tip and the flange wall, evolved from uniaxial stretching to near plane strain, respectively. They followed a linear strain path during most of the deformation process, except at the last step, where they exhibited certain lack of proportionality. Point B, located at the flange wall, experienced a significant non-proportional strain path, starting in biaxial stretching and ending in uniaxial stretching. Finally, Point A, located at the die radius, underwent severe compression and followed a linear path.

According to the above results, a clear non-proportionality in the strain paths was observed for the points in the flange wall away from the edge. However, the strain paths tended to become proportional at the flange edge zone, reaching a complete proportionality at the exact hole edge. Thus, since the strains in the region near the flange edge that exceeded the conventional FLC followed almost linear paths, non-proportional strain path effects cannot account for why failure did not occur in this region.

3.3.2 *Bending effect*

It is very well known that bending induced by forming tools has a beneficial effect on formability because it enables higher strains at the sheet surface before the onset of localized necking. The bending effect and its contribution in the enhancement of formability in press-working (see, e.g., Vallellano et al. [26,27], Luo and Wierzbicki [28], Morales-

Palma et al. [29] and Neuhauser et al. [30]) and incremental sheet-forming processes (see, e.g., Silva et al. [31] and Centeno et al. [32]) have been widely discussed in this research field.

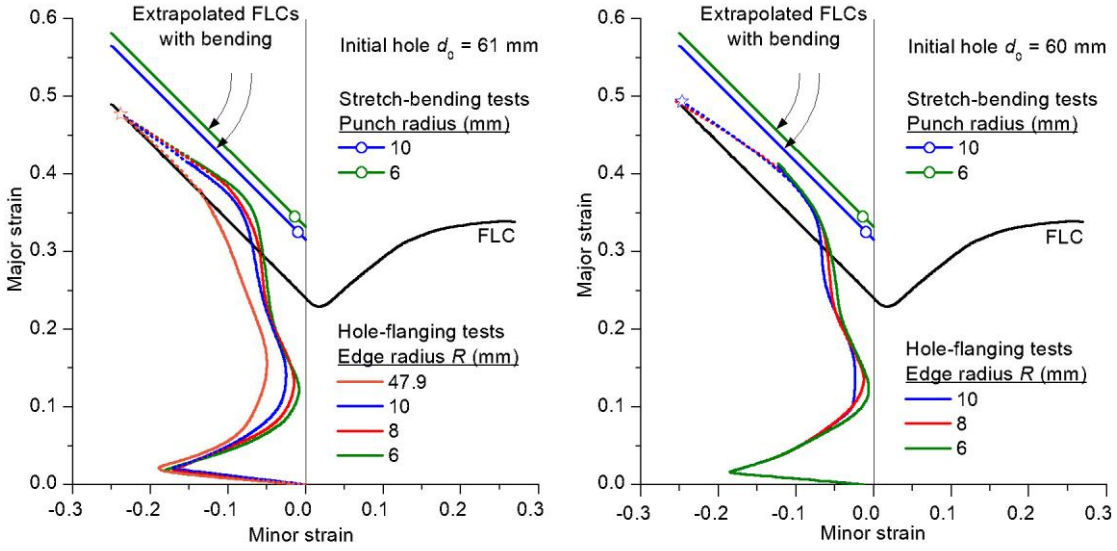

Figure 9. In-plane principal strains distribution along the meridional direction for hole-flanged parts with different punch edge radii and pre-cut holes of 61-mm (successful flange) and 60-mm diameter (necked flange). Comparison with the results for stretch-bending tests using cylindrical punches with a 6 and 10-mm radius and the extrapolated FLC with the bending contribution.

Figure 9 shows the in-plane strain distributions along the meridional direction for the hole-flanging tests with 61 and 60-mm pre-cut hole diameters and the different punch edge radii. The first graph corresponds to the minimum pre-cut hole diameter needed to fabricate a successful flange, and the second graph corresponds to the maximum pre-cut hole that is necessary to obtain a flange that is necked at the hole tip.

To quantify the effect of bending, a series of stretch-bending tests was developed using cylindrical punches with a 10 and 6-mm radius, which corresponded, respectively, to the maximum and minimum edge radii in the cylindrical hole-flanging punches. Both forming limit strains from the stretch-bending tests are depicted in Figure 9 near the plane strain. Assuming a constant thickness strain during the appearance of necking, from these limit strains, two lines parallel on the left-hand side of the FLC were extrapolated through the uniaxial region in the principal strain diagram. For our purposes, these lines may be considered as a rough estimation of the FLCs with the bending contribution. As expected, the smaller the bending radius was, the higher the estimated FLC values was. However, as shown, the differences between the 6 and 10-mm radius results were not very significant.

As seen, the strain distributions for all cylindrical punches in Figure 9 are below their estimated FLCs with bending, indicating that failure by necking was not expected to occur in the flange wall. When the influence of bending disappeared, very near the hole edge, the conventional FLC again dominated the failure of the sheet. In fact, the flanges finally failed in this zone (see the results for the 60-mm pre-cut hole diameter).

4. Numerical simulation

In order to confirm that bending plays an important role in the apparent local enhancement of formability exhibited by the material in hole flanging, a numerical simulation has been performed using the commercial finite element (FE) code Abaqus®/Standard. The FE model reproduces the experimental test using a punch edge radius of 6 mm, a die edge radius of 3 mm and a pre-cut hole diameter of 61 mm. It has been simplified defining a 2D-axisymmetric model and assuming the Hill's anisotropic yield criterion. The simulation aims to reveal the strain gradients through the flange thickness.

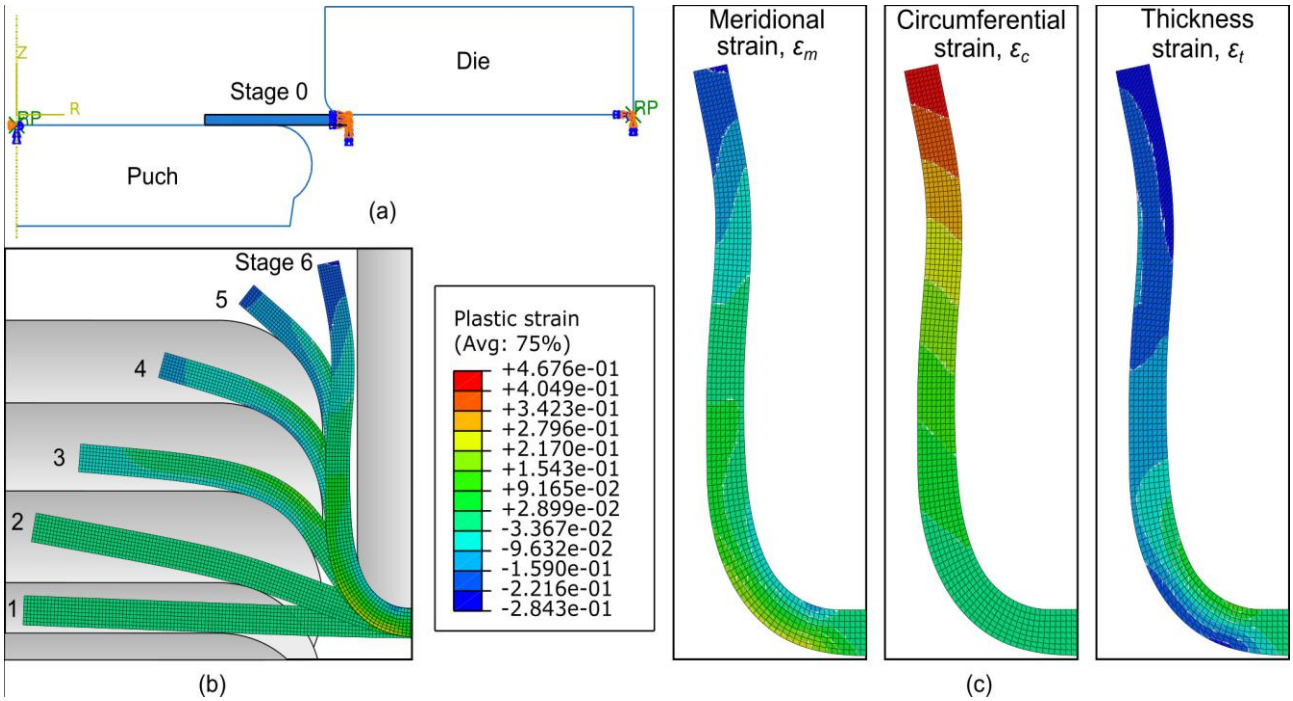

Figure 10. Numerical simulation of a hole-flange operation: (a) FE model definition; (b) evolution of the deformed flange; and (c) distribution of principal strains on thickness in the final flange.

Figure 10(a) shows the FE model. The sheet blank was modelled using axisymmetric shell elements of size 0.2×0.2 mm. All the degrees of freedom of the nodes located at the outer edge of the blank were fixed in order to simulate the effect of the blank holder. The forming tools were modelled as analytical rigid surfaces. The mechanical properties of the AA7075-O sheets of 1.6-mm thickness are summarized in Table 1. A Hollomon type law $\sigma = 314 \cdot \varepsilon^{0.13}$ MPa was used to describe the hardening behaviour of the aluminium alloy, as recently described by the authors [33,34]. The sheet blank was meshed with 944 square elements of size 0.2 mm. A surface-to-surface contact algorithm with the finite sliding formulation was used and a Coulomb's friction coefficient of 0.1 was assumed.

The evolution of the flange deformation is depicted in Figure 10(b) at stages 1 to 6. Stages 1 and 2 show that the flange has been separated from the flat punch and it has not yet been adapted to the punch edge geometry. It should be noted that the hole edge separation from the punch seems to be slightly overestimated compared to the experimental

observation. Stages 3 to 6 simulate the flange geometry of interrupted tests 1 to 4 shown in Figure 8, respectively. Notice that the bent flange is well adapted to the punch edge geometry in stages 3 to 5. From stage 5, the hole edge continues to bend without adapting to the punch shape. As can be observed, the simulation reproduces fairly well the geometry of the specimens in interrupted tests.

The strain distributions of the final flange along the meridional, circumferential and thickness directions are illustrated in Figure 10(c). The coloured scale of the legend is the same for the three principal strains. As seen, the flange stretching is positive in the circumferential direction and negative in the meridional and thickness directions. These distributions also reveal the strain gradients through the thickness: the outer surface of the flange is more stretched circumferentially and less stretched in the other two directions than the inner surface.

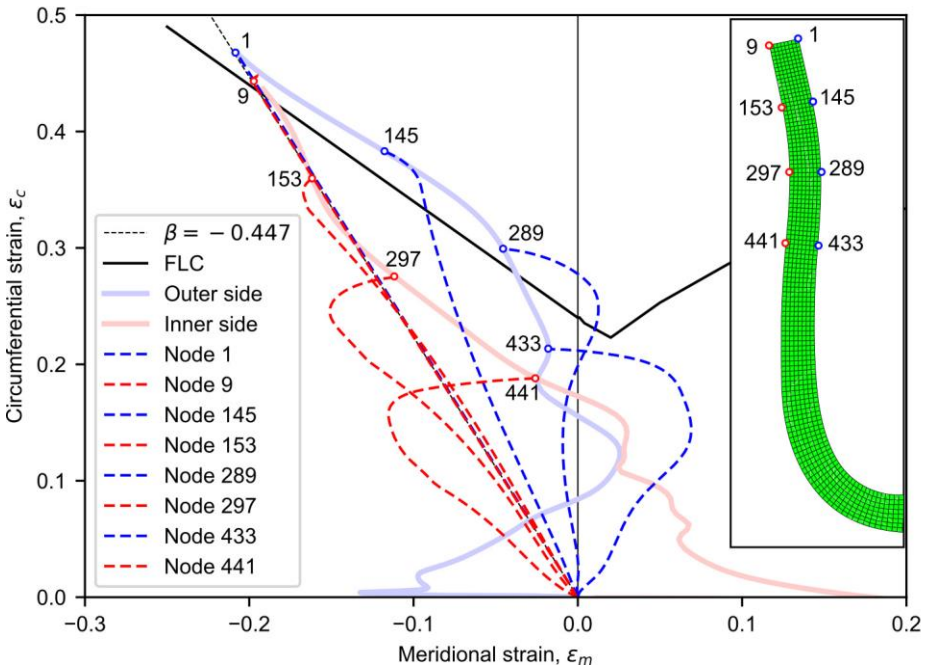

Figure 11. Strain paths and strain distributions along the flange in the outer and inner surfaces.

Figure 11 depicts the strain distribution along the outer and inner surfaces of the final flange as well as the strain paths of the 8 nodes depicted in the flange section. The diagram presents strains in the circumferential and meridional directions. As can be seen, the strain paths of the 4 nodes in the outer surface and the final strain distribution in the same surface reproduce reasonably well the tendency of the experimental FLD represented in Figure 8. In particular, notice the linear part of the strain path of the node 145 that exceeds clearly the FLC according to the experimental observations. It can be also observed that the simulated flange wall stretches less in the meridional direction (ε_m more negative) than the real wall. This small deviation seems to be directly related to the aforementioned separation of the hole edge with the flat zone of the punch and, therefore, is attributed to the material modelling.

The bending effect can be again understood by analysing the final strain distribution along the inner sheet surface. As can be seen in Figure 11, final strains near the flange edge (nodes 153 and 297) are well below of the FLC, and thus the plastic instability through the sheet thickness in this zone has been delayed and the conventional FLC should not be

used. Regarding the strain paths in both sheet surfaces, it can be observed that strain gradients through the thickness increase as the material away from the flange edge is in contact with the punch edge (bending) and afterwards decrease (unbending), see e.g. the pairs of nodes 289-297 and 433-441.

5. Conclusions

The formability of hole-flanged parts fabricated using press-working was analysed via the *LFR* and the conventional FLC. The influence of the punch profile on the deformation process and flange failure was discussed in detail. A series of conventional hole-flanging tests using 1.6-mm 7075-O aluminium alloy sheet were performed using three cylindrical punches with different edge radii and a hemispherical punch. The process deformation was also simulated numerically to support the formability analysis. The main conclusions of this study can be summarised as follows:

- The failure mode prevailing at the formability limit was the initiation of necking at the edge of the flange.
- For the successful parts fabricated with cylindrical punches with bending ratios ranging from 0.16 to 0.27, the heights of the flanges were nearly identical for a given pre-cut hole (d_0). The hemispherical punch produced slightly lower flanges.
- The *LFR* is a good measure of the formability in conventional hole-flanging operations because this parameter directly quantifies the maximum stretching of the material at the hole tip, where failure occurs in practice. The *LFR* remained constant with *R* and was equal to 1.57.
- In general, conventional FLC was not a suitable tool for analysing the formability of the material along the flange, except at the flange tip.
- The distribution of the principal strains on the outer side of the flange showed a 2-shaped curve. Except for the hemispherical punch, the strain curves for the successful hole-flanged parts near the formability limit were clearly above the FLC, but failure did not occur. This event was observed in the flange wall near the edge. Two aspects of the deformation history were a priori candidates for explaining this inability of the conventional FLC to describe the failure during hole flanging by press-working: the non-proportionality of the strain path and the bending induced by the punch edge radius. Experimental and numerical analysis corroborate that the bending effect was the main factor that controlled the apparent enhancement of formability in the flange wall near the edge, which was clearly influenced by the punch profile. Far from the flange edge, the strain paths were considerably more non-proportional.
- The punch corner radius mainly affected the final value of the meridional strain, i.e., the minor principal strains along the flange. A smaller punch edge radius induced a shift in the strain curves to the right in the principal strain diagram. This shift was responsible for the lower value in the flange height exhibited by the semi-spherical punch.
- The condition for the onset of localized necking at the flange tip was fulfilled at the intersection of the FLC with the line of pure uniaxial tension. Accordingly, the *LFR* value was associated with this intersection point. This

explains why the *LFR* is a material constant and independent of the punch profile. This can be obtained as $LFR = exp(\varepsilon_{1,UT}^{*})$, where $\varepsilon_{1,UT}^{*}$ is the major strain at the onset of localized necking in the sheet under pure uniaxial tension.

Compliance with ethical standards

Funding: This research was funded by the Spanish Government throughout research project DPI2015-64047-R.

Conflict of interest: M. Borrego has received research grant BES-2013-063796 from Spanish Government. The rest of authors declare that they have no conflict of interest.

References

[1] Yamada Y., Koide M. (1967). Analysis of the bore-expanding test by the incremental theory of plasticity. International Journal of Mechanical Sciences 10: 1–14.

[2] Johnson W., Chitkara N.R., Minh H.V. (1977). Deformation modes and lip fracture during hole flanging of circular plates of anisotropic material, Trans. ASME J. Eng. Ind. 99: 738–748.

[3] Tang S.C. (1981). Large elasto-plastic strain analysis of flanged hole forming. Computers and Structures 13: 363–370.

[4] Levy B.S., Van Tyne C.J. (2008). Failure During Sheared Edge Stretching. J. Mater. Engng. Perform. 17(6):842–848.

[5] Pathak N., Butcher C., Worswick M. (2016). Assessment of the Critical Parameters Influencing the Edge Stretchability of Advanced High-Strength Steel Sheet. J. Mater. Engng. Perform. 25(11):4919–4932.

[6] Kumagai T. and Saiki H. (1998). Deformation Analysis of Hole Flanging with Ironing of Thick Sheet Metals, Metals and Materials 4: 711-714.

[7] Leu D.K., Chen T.C., Huang Y.M. (1999). Influence of punch shape on the collar-drawing process of sheet steel. Journal of Materials Processing Technology 88: 134–146.

[8] Huang Y.M., Chien T.C. (2001). Influence of the punch profile on the limitation of formability in the hole-flanging process. Journal of Materials Processing Technology 113: 720–724.

[9] Huang Y.M., Chien K.H. (2001). The formability limitation of the hole-flanging process. Journal of Materials Processing Technology 117: 43–51.

[10] Krichen A., Kacem A., Hbaieb M. (2011). Blank-holding effect on the hole-flanging process of sheet aluminum alloy. Journal of Materials Processing Technology 211: 619–626.

[11] Kacem A., Krichen A., Manach P.Y. (2014). Prediction of damage in the hole-flanging process using a physically based approach. International Journal of Damage Mechanics 24: 840–858.

[12] Kacem A., Krichen A., Manach P.Y. (2015). Finite element analysis of hole-flanging process with various anisotropy assumptions. International Journal of Advanced Manufacturing Technology 80: 11–19.

[13] Soussi H., Masmoudi N., Krichen (2016). A. Analysis of geometrical parameters and occurrence of defects in the hole-flanging process on thin sheet metal, Journal of Materials Processing Technology 234: 228–242.

[14] Yoon J. I., Jung J., Lee H. H., Kim G.-S., Kim H. S.(2016). Factors governing hole expansion ratio of steel sheets with smooth sheared edge, Met. Mater. Int. 22: 1009-1014.

[15] Yoon J. I., Jung J., Kim J. G., Sohn S. S., Lee S., Kim H. S. (2017). Key factors of stretch-flangeability of sheet material, J. Mater. Sci. 52: 7808-7823.

[16] Wang K., Luo M., Wierzbicki T. (2014). Experiments and modeling of edge fracture for an AHSS sheet. Int. J. Fract. 187:245–268.

[17] Silva M.B., Teixeira P., Reis A. (2013). On the formability of hole-flanging by incremental sheet forming. J Mater Des Appl 227: 91–99.

[18] Montanari L., Cristino V.A., Silva M.B., Martins P.A.F. (2013). On the relative performance of hole-flanging by incremental sheet forming and conventional press-working. Proc IMechE Part L: J Materials: Design and Applications, 1–11.

[19] Cristino V.A., Silva M.B., Martins P.A.F. (2015). Hole-flanging of metals and polymers produced by single point incremental forming. Int. J. Materials and Product Technology 50: 37-48.

[20] Borrego M., Morales-Palma D., Martínez-Donaire A.J., Centeno G., Vallellano C. (2016). Experimental study of hole-flanging by single-stage incremental sheet forming. Journal of Materials Processing Technology 237: 320–330.

[21] Martínez-Donaire A.J., García-Lomas F.J., Vallellano C. (2014). New approaches to detect the onset of localised necking in sheets under through-thickness strain gradients. Materials and Design 57: 135–145.

[22] Graf A., Hosford W. (1994). The influence of strain-path changes on forming limit diagrams of Al 6111T4. International Journal of Mechanical Sciences 36: 897–910.

[23] Stoughton, T.B., Yoon J.W. (2012). Path independent forming limits in strain and stress spaces. International Journal of Solids and Structures 49: 3616–3625.

[24] Barata da Rocha, Barlat F., Jalinier J.M. (1985). Prediction of the forming limit diagrams of anisotropic sheets in linear and non-linear loading. Materials Science and Engineering 68: 151–164.

[25] Yoshida K., Kuwabara T., Kuroda M. (2007). Path-dependence of the forming limit stresses in a sheet metal. Int. J. Plast. 23: 361–384.

[26] Vallellano, C., Morales, D., García-Lomas, F.J. (2008). A study to predict failure in biaxially stretched sheets of aluminum alloy 2024-T3. Materials and Manufacturing Processes 23: 303-310.

[27] Vallellano, C., Morales, D., Martinez, A.J., Garcia-Lomas, F.J. (2010). On the use of concave-side rule and critical-distance methods to predict the influence of bending on sheet-metal, International Journal of Material Forming, 3 (suppl. 1): 1167-1170.

[28] Luo M., Wierzbicki T. (2010). Numerical failure analysis of a stretch-bending test on dual-phase steel sheets using a phenomenological fracture model. International Journal of Solids and Structures 47: 3084–3102.

[29] Morales-Palma D., Vallellano C., García-Lomas F.J. (2013). Assessment of the effect of the through-thickness strain/stress gradient on the formability of stretch-bend metal sheets. Materials and Design 50: 798–809.

[30] Neuhauser F. M., Terrazas O., Manopulo N., Hora P., Van Tyne C. (2018). The bending dependency of forming limit diagrams. Int. J. Mater. Form. https://doi.org/10.1007/s12289-018-1452-1.

[31] Silva M.B., Nielsen P.S., Bay N., Martins P.A.F. (2011). Failure mechanisms in single point incremental forming of metals. International Journal of Advanced Manufacturing Technology 56: 893–903.

[32] Centeno G., Bagudanch I., Martínez-Donaire A.J., García-Romeu M.L., Vallellano C. (2014). Critical analysis of necking and fracture limit strains and forming forces in single-point incremental forming. Mater. Des. 63: 20–29.

[33] Morales-Palma D., Borrego M., Martínez-Donaire A. J., Centeno G., Vallellano C. (2018). Optimization of Hole-Flanging by Single Point Incremental Forming in Two Stages. Materials 11, 2029. https://doi.org/10.3390/ma11102029.

[34] Martínez-Donaire A. J., Borrego M., Morales-Palma D., Centeno G., Vallellano C. (2019). Analysis of the influence of stress triaxiality on formability of hole-flanging by single-stage SPIF. Int. J. Mech. Sc. 151: 76-84 https://doi.org/10.1016/j.ijmecsci.2018.11.006.